RSC Advances

ROYAL SOCIETY OF CHEMISTRY

www.rsc.org/advances

RSC Advances

RSCPublishing

ARTICLE

Graphene-modified $BiMo_{0.03}V_{0.97}O_4$ thin-film photoanode for enhanced photoelectrochemical water splitting performance

Cite this: DOI: 10.1039/x0xx00000x

Received 00th January 2012,
Accepted 00th January 2012

DOI: 10.1039/x0xx00000x

www.rsc.org/

Weibing Li[a], Jiguang Yue[a], Yuyu Bu[b], Zhuoyuan Chen*[b]

In this study, graphene is coated on the surface of the Mo-doped $BiMo_{0.03}V_{0.97}O_4$ (BiMoVO) film by the galvanostatic reduction deposition. The BiMoVO/graphene (BiMoVO/G) thin-film photoanode exhibits the optimal photoelectrochemical performance with the graphene deposition time of 600 s. The photoinduced current density is 3.5 $mA \cdot cm^{-2}$ at the bias potential of 1 V, which increases by approximately 2.3 times of that of the BiMoVO thin-film photoanode. Moreover, the BiMoVO/G photoanode shows higher photoelectrochemical stability as well. The improvement of the photoelectrochemical property is attributed to the graphene coating, which acts as the receptor of the photogenerated electrons from the BiMoVO film. Therefore, the photogenerated electrons can be rapidly transferred to the substrate through the graphene channel, enhancing the separation efficiency of the photogenerated electron–hole pairs and prolonging the lifetime of the photoinduced electrons.

Introduction

Photoelectrochemical technique is widely considered as one of the key technologies to solve the energy crisis and environmental pollution problems[1-6]. The enhancement of the quantum yield and the optimization of the materials with photoelectric conversion capabilities are the keys for pushing this technique into practical application. Three properties are needed for the photoelectrochemical materials. Firstly, the materials should have sufficiently wide light absorption range and absorption intensity to capture photons as much as possible. Secondly, the materials should have high electron mobility and less bulk traps during the migration process of photogenerated electrons and holes from the interiors of the materials to their surfaces. Finally, the redox capability of the photoinduced electrons and holes generated by these materials should be high enough. If any of the above mentioned properties of the materials cannot meet the requirements, the photoelectrochemical performance of the materials will be decreased[7,8]. Thus, it is necessary to modify the surface or the interface of the materials to enhance their photoelectrochemical performance.

Since Novoselov *et al.*[9] reported that graphene was a two-dimensional ultrathin planar-structure carbon material in 2004, wide attentions have been attracted from the researchers due to its excellent luminous, electrical, thermal and magnetic effect[10-13]. In the fields of photocatalytic or photoelectrochemical materials, novel graphene based semiconductor composite materials are widely considered as highly promising solar energy conversion materials[14-17]. Numerous studies indicate that the enhancement of the photocatalytic or photoelectrochemical performance of the graphene/semiconductor materials composites mainly come from the following four aspects: (1) With the formation of the heterojunction electric field between graphene and semiconductor materials, the separation efficiency of

photogenerated electrons and holes are efficiently enhanced. (2) By loading the graphene on the surface of other semiconductor materials, the migration rate of photogenerated electrons can be enhanced and the lifetime of photogenerated electrons can be prolonged. (3) Graphene, acted as the surface co-catalyst of the semiconductor materials, can enhance the redox capability of the photoinduced electrons and holes generated by the semiconductor materials. Williams *et al.*[18] mixed TiO_2 with graphene oxide and subsequently prepared TiO_2/graphene composite materials by photo-assisted reduction. They showed that the photocatalytic activity of TiO_2 can be significantly enhanced by compositing graphene with TiO_2. Xu *et al.*[19] loaded graphene on the surface of ZnO nanoparticles and they found that the photocatalytic performance could be significantly enhanced after composting 2 wt% graphene with ZnO. The main principle is that the existence of graphene accelerates the migration of photogenerated electrons and thus efficiently inhibits the recombination of photogenerated electrons and holes. Zhang *et al.*[14] loaded Ag@AgCl on the surface of graphene. The separated photoinduced electrons, generated by the surface plasma resonance effect of Ag, swiftly transferred to graphene and reacted with the surrounding media. Kim *et al.*[20] smashed large pieces of graphene into nano-scale pieces, and subsequently assembled on the surface of TiO_2 to prepare graphene@TiO_2 shell-core structure material. They found that the increased contact area between TiO_2 and graphene could increase the interface heterojunction electric field area and thus efficiently enhanced the separation efficiency of the photogenerated electrons and holes. Iwase *et al.*[21] prepared all-solid $BiVO_4$/graphene/$SrTiO_3$ Z-scheme photocatalyst and found that graphene could act as the efficient electron-transfer medium. Under visible light illumination, this photocatalyst could split water completely. Song *et al.*[22] assembled graphene oxide on the surface of TiO_2 nanorod array and found that the graphene oxide coated on the surface of TiO_2 nanorod could enhance the photoelectric conversion performance of the TiO_2 nanorod array to some extent. Liu *et al.*[15] prepared graphene on the surface of TiO_2 nanorod array by cyclic voltammetry technique and found that the coated graphene could enhance the mobility of the photogenerated electrons and extend the light absorption range of the composite material to visible light region.

Polymetallic oxide monoclinic $BiVO_4$ is a stable, low-cost and environment-friendly semiconductor material with the band gap of 2.4 eV and possesses the ability to absorb visible light[23-27]. Relevant studies have shown that the theoretical photoelectric conversion efficiency of this material can reach 9.1 %[28]. Therefore, the usage of this material in the area of photocatalysis or photoelectrochemical splitting water is always attracting attention of researchers. Because the conduction band potential of $BiVO_4$ is slightly more positive than the reduction potential of water, hydrogen production from water splitting under zero bias potential using this material cannot be achieved. However, it has relatively positive valance band potential, which makes it be an excellent material for photoelectrochemical oxidizing water to produce oxygen. To improve the performance of photoelectrochemical oxidizing water, numerous modifying works for $BiVO_4$ have been performed by the researchers in recent years. Studies indicate that doping elements[29,30], constructing heterojunction electric field with semiconductors[31], surface modification[7,23] and preparing mesoporous $BiVO_4$[32] can efficiently enhance the photoelectrochemical oxidizing water performance of $BiVO_4$. The photocatalytic or photoelectrochemical properties can be enhanced to a large extent by compositing $BiVO_4$ with graphene. Sun *et al.*[33] firstly synthesized ordered monoclinic $BiVO_4$ quantum tubes, and subsequently loaded on graphene to prepare $BiVO_4$ quantum tubes-graphene composite photocatalyst. They found that the optimization of $BiVO_4$ nanostructure and the loading of graphene can significantly enhance the visible light-driven photocatalytic properties of $BiVO_4$. Ng *et al.*[34] firstly prepared $BiVO_4$ and $BiVO_4$/Graphene composite powder materials. The powder was then made into slurry and coated on the F-doped SnO_2 (FTO)

conductive glass by dip-coating method to prepare thin-film photoelectrodes. They found that the mixing of graphene and $BiVO_4$ benefitted the transfer of photogenerated electrons to FTO substrate, leading to the enhancement of the photoelectrochemical performance. However, in the film prepared by dip-coating method, the connections between $BiVO_4$ particles were pretty loose, which inhibited the transferring process of photogenerated electrons. On the other hand, the intrinsic photoelectric conversion performance of the unmodified $BiVO_4$ is poor. Therefore, the monochromatic incident photon-to-electron conversion efficiency (IPCE) of this composite photoelectrode in the wavelength range of 300~500 nm did not exceed 5 %. Thus, it has important significance to further enhance the photoelectrochemical performance of the $BiVO_4$-graphene composite photoelectrode.

Based on the above-mentioned reasons, in the present work, the authors prepared Mo-doped $BiMo_{0.03}V_{0.97}O_4$ (BiMoVO) thin-film photoanode on the surface of FTO by the pyrolysis of organic materials. Luo et al.[30] have prepared Mo doping $BiVO_4$ photoanode, the research results indicated that the photoelectrochemical water oxidation performance was improved greatly when the doping amount reached 3 %. So, in this study, we have choose the $BiMo_{0.03}V_{0.97}O_4$ as a photoelectrode. And then, the galvanostatic reduction deposition method was used to prepare graphene coating layer on the BiMoVO film. The aim was to enhance the photoelectrochemical water splitting performance of the prepared BiMoVO/graphene (BiMoVO/G) composite film by using the dual roles from Mo doping and graphene modifying.

Results and discussion

Figure 1 shows the XRD patterns of the prepared samples. As shown in the XRD pattern of the BiMoVO film, the intensive diffraction peaks at 19.5°, 29° and 30.5° were observed, corresponding to the monoclinic phase of the prepared BiMoVO film with a high crystallinity. Tokunaga *et al.*[35] reported that the BiMoVO film with monoclinic phase showed the optimal photocatalytic oxygen reduction property. In the XRD pattern, no other impurity peaks were observed except the diffraction peak of the FTO conducting glass, indicating that a small amount of doped Mo did not affect the monoclinic phase structure of $BiVO_4$ film. By Comparing the XRD pattern of BiMoVO with the BiMoVO/G composites with different graphene deposition time, there was no difference of the monoclinic phase, indicating that the deposition of graphene did not affect the crystal structure of BiMoVO.

The characteristic diffraction peaks from graphene were not observed in the XRD patterns of the BiMoVO/G composites, as shown in Figure 1. When the graphene deposition time is larger than 700 s, a slight heave was observed in the range of 20°-30°, which could probably be caused by the deposition of the graphene. However, this cannot be entirely sure. Therefore, XPS was further used to analyze the BiMoVO/G composites to confirm the deposition of graphene on the surface of the BiMoVO film. Figure 2 shows the XPS results of the BiMoVO-600 composite. As shown in Figure 2a, the prepared sample was composed of Bi, Mo, V, O, and C, and the electron peak of Sn was from the FTO substrate. Figure 2b shows the high-resolution XPS core level spectrum of C1s. The curve fitting demonstrates that the C in the sample existed mainly in the form of the C–C bond (Peak area rate 97%), and the peaks corresponding to the oxidation state of the C–O (Peak area rate 2.5%) and O–C=O (Peak area rate 0.5%) bonds were relatively weak, indicating that the graphene on the surface of the BiMoVO film was highly reduced. In addition, the XPS results of the other elements are shown in Figure S1.

Figure S2 shows the FTIR spectra of the BiMoVO and BiMoVO/G-600 films. A wide peak at 1500 cm^{-1} was observed in the spectrum of the BiMoVO film (Curve a). After the deposition of graphene, the C–C and C–O vibration peaks were obviously observed, as shown in the spectrum of the BiMoVO/G-600 film (Curve b), confirming that the graphene was deposited on the surface of BiMoVO.

Figure 3 shows the SEM morphologies of the BiMoVO and BiMoVO/G-600 thin films under low and high magnifications. Figure 3a shows the surface morphology of the BiMoVO film under low magnification. Accordingly, the particles in the BiMoVO film distributed homogeneously, and a certain space existed among them. Figure 3b shows the surface morphology of the BiMoVO film under high magnification, and the particle size is approximately 500 nm with irregular shapes. Figure 3c shows the SEM morphology of the BiMoVO/G-600 film, and the particles in the sample were homogeneously distributed as well. However, the space among the particles obviously decreased compared to that shown in Figure 3a, probably caused by the deposition of the graphene. The inset in Figure 3c is the cross-sectional view of the BiMoVO/G-600 thin film, indicating a layer of the BiMoVO/G film with a thickness of 500 nm homogeneously deposited on the FTO conductive glass. Figure 3d shows the SEM morphology of the BiMoVO/G-600 film under high magnification, and a layer of coated graphene was observed on the surface of the BiMoVO film, further confirming that the graphene was successfully deposited on the surface of the BiMoVO film. The inset in Figure 3d is the TEM image of the BiMoVO/G-600 thin film. From this image we can find that the BiMoVO is clad by graphene thin film uniformly.

The particle size of BiMoVO/G is approximately 500 nm, as shown in Figure 3b. The thickness of the BiMoVO/G film deposited on the FTO surface is also approximately 500 nm. Thus, the BiMoVO/G film is mainly composed of a single BiMoVO/G particle layer. After the BiMoVO particles were covered by the graphene, the BiMoVO particles contact with both the FTO film and the graphene, resulting in the formation of an effective electron transfer path.

Figures S2a and S2b show the SEM morphologies of the BiMoVO/G-400 film under low and high magnifications, respectively. A certain amount of graphene was deposited on the BiMoVO film after 400-s deposition of graphene. The space among the particles in Figures S2a and S2b was relatively bigger than that shown in Figures 3c and 3d, indicating that less amount of graphene was deposited on the BiMoVO/G-400 film than on the BiMoVO/G-600 film. Figures S2c and S2d show the SEM morphologies of the BiMoVO/G-800 film. A large amount of graphene was coated on the surface of the BiMoVO film, and the space among the particles was filled with graphene. Therefore, the deposition time can be used to control the amount of graphene on the BiMoVO film.

Figure 4 shows the UV/Vis diffuse reflectance spectra of BiMoVO and the BiMoVO/G films after different graphene deposition time. As shown in Figure 4, the absorption thresholds of the samples were at around 520 nm, indicating that the deposition of graphene did not increase the optical absorbance of the BiMoVO film. The amount of deposited graphene affected the absorption at the wavelength <520 nm. Because of the intrinsic absorption of the graphene, the absorption at >520 nm increased with the increase of the amount of the deposited graphene[16,18-19].

The properties of the BiMoVO and BiMoVO/G photoanodes were further investigated by the photoelectrochemical and electrochemical measurements, and the results are shown in Figure 5. Figure 5A shows the i–t curve of the BiMoVO and BiMoVO/G photoanodes. The photoinduced current density of the BiMoVO photoanode was 1.5 $mA \cdot cm^{-2}$, and it increased with the increase of the graphene deposition time. The photoinduced current density reached 3.5 $mA \cdot cm^{-2}$ at the graphene deposition time of 600 s, which increased 2.3 times compared to that of the BiMoVO photoanode, indicating that the deposition of graphene on the BiMoVO film significantly improved the photoinduced current densities of the BiMoVO/G photoanodes. With the further increase of the graphene deposition time, the photoinduced current densities decreased. Figure 5B shows the i–V curves of the BiMoVO and BiMoVO/G photoanodes. The photoanodes generated small photoinduced current densityies at the scanning voltages around 0 V, and the photoinduced current densities slightly increased with the further increase of the scanning potential. When the scanning potential is larger than 0.4 V, the photoinduced current densities are rapidly increased. The relatively high onset potential of the photoinduced current indicates that the positive conduction band potential of the BiMoVO film decreases the reducibility of the photogenerated electrons, and much more positive bias potential is required to transfer this kind of photogenerated electrons to the FTO conductive galss. The photoinduced current densities of the BiMoVO/G photoanodes were significantly higher than that of the BiMoVO photoanode under the same bias potential. The BiMoVO/G-600 photoanode shows the highest photoinduced current density (6.5 $mA \cdot cm^{-2}$ at the bias potential of 1.5 V). Figure 5C shows the IPCE curves of the BiMoVO and BiMoVO/G-600 photoanodes at the bias potential of 1 V (vs Ag/AgCl). The photoelectric conversion efficiency for the BiMoVO photoanode maintained at around 40% under the illumination of the incident light <420 nm. However, this value decreased rapidly at wavelengths >420 nm. For the BiMoVO/G-600 photoanode, the photoelectric conversion efficiency was maintained at around 50% under the illumination of the incident light <440 nm. And this value decreased rapidly at wavelengths >440 nm. Moreover, the BiMoVO/G-600 photoanode showed higher photoelectric conversion efficiency compared to that of the BiMoVO photoanode in the wavelength range of 440–520 nm. To verify the photoelectrochemical stability of the BiMoVO/G-600 photoanode, the i–t curve was measured under long time (10 h) of illumination, and the results are shown in Figure 5D. The photoinduced current density of the BiMoVO/G-600 film firstly decreased, then increased, and finally decreased slowly under the long-term illumination. The photoinduced current density was maintained at around 3.2 $mA \cdot cm^{-2}$, decreased by 8.6% compared to the initial value (3.5 $mA \cdot cm^{-2}$) after 10 h of visible light illumination, indicating that the photoanode had relatively high photoelectric conversion stability.

PL spectroscopy and EIS were further used to investigate the mechanism of the improvement in the photoelectrochemical water splitting performance induced by the deposition of graphene on the BiMoVO film, and the results are shown in Figure 6. Figure 6A shows the PL spectra of the BiMoVO and BiMoVO/G photoanodes. Semiconductor materials can generate separated photoinduced electrons and holes under illumination of incident light with suitable wavelength. The recombination of the separated electrons and holes will convert into heat or fluorescence. The intensity of the fluorescence is proportional to the recombination rate of the electrons and

holes, i. e., the more intensive fluorescence, the more vigorous recombination of the photoinduced electrons and holes and the shorter lifetime of the photogenerated electrons. As shown in Figure 6A, the BiMoVO film had the most intensive fluorescence emission, and the fluorescence was quenched by the deposition of graphene on the film, indicating that the graphene efficiently prevented the recombination of the photogenerated electrons and holes and increased the lifetime of the photogenerated electrons, probably caused by the high electron capturing capability and electron transferring ability of the graphene. Figure 6B shows the EIS result of the BiMoVO and BiMoVO/G-600 photoanodes in 0.1 M Na_2SO_4 neutral electrolyte in the dark. We have fitted the EIS curves by a simple Randles Circuit which is inset in Figure 6B. The fitted values were showed in Table 1. The results demonstrate that the resistance value of the BiMoVO film was 5017.34 Ω cm^2, and the value decreased to 3392.27 Ω cm^2 after depositing graphene on BiMoVO, indicating that graphene may provide the electron migration channel for the film. Consequently, the recombination probability decreased since the electrons could be transferred to the substrate under a lower resistance, which increased the lifetime of the electrons, and eventually improved the efficiency of the photoelectrochemical water splitting performance.

Figure 7 shows the possible mechanism of the improvement of the photoelectrochemical water splitting performance using the BiMoVO/G photoanode. BiMoVO absorbed photon, and the electrons in the valence band were excited to the conduction band under visible light. Graphene is an efficient electron receptor; therefore, the photogenerated electrons from the BiMoVO film were rapidly transferred to graphene, and then the electrons were further transferred to the FTO conductive glass at the bias potential of 1 V, and finally hydrogen was produced on Pt by the reduction of water. The photogenerated holes could transfer to the surface of the BiMoVO film and reacted with water on the surface of the film uncoated with graphene to produced oxygen. The rapid transfer of the photogenerated electrons through graphene effectively decreased the secondly recombination probability of the photoinduced electrons and holes, thus improving the efficiency of the photoelectrochemical water splitting.

Experimental

1 Preparation of BiMoVO and BiMoVO/G composite

BiMoVO precursor solution was prepared based on the method of Luo *et al.*[24] and the specific steps were as follows. Firstly 0.3492 g of bismuth nitrate pentahydrate was ultrasonically dissolved into 3.6 mL of acetic acid. Afterwards, 0.2386 g of vanadium acetylacetonate and 0.007 g of molybdenum acetylacetonate were ultrasonically dissolved into 23.3 mL of acetylacetone. Then, the above two solution were mixed and ultrasonically dispersed for 30 min. After the sonication, the mixed solution was treated by standing and aging for 24 h to obtain BiMoVO precursor solution.

The BiMoVO film was prepared by the following method. Firstly a uniform precursor film was coated on the clean FTO conductive glass with the area of 1×1.3 cm^2 by spin coating method (2000 r·Min^{-1}, 20 s). The uniform ultrathin BiMoVO film was obtained by further annealing in air atmosphere under 470 °C for 30 min (heating/cooling rate was 10 °C·Min^{-1}). To increase the thickness of the BiMoVO film, 10 μL precursor solution was uniformly coated on the surface of the prepared ultrathin BiMoVO film for each time, followed by annealing under 470 °C for 30 min. The above process was repeated for 6 times and the BiMoVO film with the thickness of approximately 500 nm was obtained. Dilute hydrochloric acid was used to dissolve the margin region with area of 1×0.3 cm^2 of the BiMoVO film to completely expose this region of FTO

conductive glass. This region of FTO conductive glass was connected with electric conductive wire by conductive silver paste and then completely sealed by epoxy resin. The final effective area of the BiMoVO film electrode was 1×1 cm^2.

The prepared BiMoVO thin-film photoelectrode was then coated with graphene by the galvanostatic reduction deposition. Firstly, 0.02 g of graphene oxide prepared by Hummer's method was ultrasonically dispersed into 50 mL of disodium hydrogen phosphate solution with the concentration of 1 $mol \cdot L^{-1}$. Three-electrode cell system was used, in which a Pt sheet, the BiMoVO thin-film electrode, and a Ag/AgCl electrode were used as the counter electrode, the working electrode, and the reference electrode, respectively, and the prepared graphene dispersion was used as the electrolyte. By using the galvanostatic reduction deposition under a constant cathodic current of 0.1 $mA \cdot cm^{-2}$, series BiMoVO/G thin-film photoelectrodes were obtained by deposition graphene for 400 s，500 s，600 s，700 s and 800 s, which were denoted as BiMoVO/G-400, BiMoVO/G-500, BiMoVO/G-600, BiMoVO/G-700 and BiMoVO/G-800, respectively.

2. Characterization of the prepared BiMoVO and BiMoVO/G composites

X-ray diffraction (XRD, D/MAX-2500/PC; Rigaku Co., Tokyo, Japan) was used to identify the crystalline structures of the prepared series photoanodes. The elementary composition and bonding information of the prepared BiMoVO/G composites were analyzed using X-ray photoelectron spectroscopy (XPS, Axis Ultra, Kratos Analytical Ltd., England). The morphologies of the prepared samples were analyzed using a scanning electron microscope (SEM, JSM-6700F; JEOL, Tokyo, Japan). A UV/Vis diffuse reflectance spectrophotometer (U-41000; HITACHI, Tokyo, Japan) was used to study the optical absorption properties of the prepared series samples. The photoluminescence (PL) intensity of the prepared photoanodes was characterized using a fluorescence spectrometer (PL, Fluoro Max-4, HORIBA Jobin Yvon, France).

3 Photoelectrochemical performance testing

A three-electrode system was employed to measure the variations of the photoinduced current density with time (i-t curve), photoinduced volt-ampere characteristic curve (i-V curve) and electrochemical impedance spectroscopy (EIS) of the prepared photoelectrodes using the CHI660D Electrochemical Workstation (Shanghai Chenhua Instrument Co., Ltd., Shanghai, China). The prepared photoelectrodes (1×1 cm^2), Ag/AgCl (saturated KCl) electrode, and platinum electrode act as the working, reference, and counter electrodes, respectively. The i-t curves were measured at a bias potential of 1 V (vs. Ag/AgCl). The i-V curves were measured from 0 to 1.5 V (vs. Ag/AgCl) with a scan rate of 0.05 $V \cdot s^{-1}$. The light source was a 150 W Xe arc lamp (PLS-SXE300, Beijing Changtuo Co. Ltd., Beijing, China) , and a 420 nm cutoff filter was used to get the visible light, with an optical intensity of 200 $mW \cdot cm^{-2}$. EIS tests were performed at open circuit potential over the frequency range between 10^5 and 10^{-2} Hz, with an AC voltage magnitude of 5 mV, using 12 points/decade. The photoelectric conversion efficiency of the photoelectrodes was studied based on their IPCE spectra, which were measured at 1 V (vs. Ag/AgCl) bais potental using a 500 W Xe lamp with a monochromator.

Conclusions

In this work, the Mo-doped $BiVO_4$ thin-film photoanode with a thickness of approximately 500 nm was prepared on the surface of FTO conducting glass by the organic pyrolysis method, and graphene was coated on the surface of the BiMoVO film via the galvanostatic reduction deposition method by controlling the graphene deposition time. The XPS, XRD, FTIR, and SEM results of the BiMoVO/G photoanode verified the deposition of graphene on the surface of the BiMoVO film. The photoelectrochemical characterizations of the BiMoVO and BiMoVO/G photoanodes prepared after different graphene

deposition time indicated that the BiMoVO/G photoanode showed much better photoelectrochemical properties than those of the BiMoVO photoanode, and the BiMoVO/G-600 photoanode showed the optimal photoelectrochemical performance. The photoinduced current density reached 3.5 $mA \cdot cm^{-2}$ at the bias potential of 1 V. Moreover, the BiMoVO/G-600 photoanode showed very high photoelectrochemical stability. The photoinduced current density decreased by only 8.6% after 10 h of visible light illumination. The results of the PL and EIS measurements demonstrate that the photogenerated electrons from the BiMoVO film can rapidly transfer to the graphene and further to the FTO conductive glass, decreasing the recombination probability of the electrons and holes and increasing the lifetime of the photoinduced electrons.

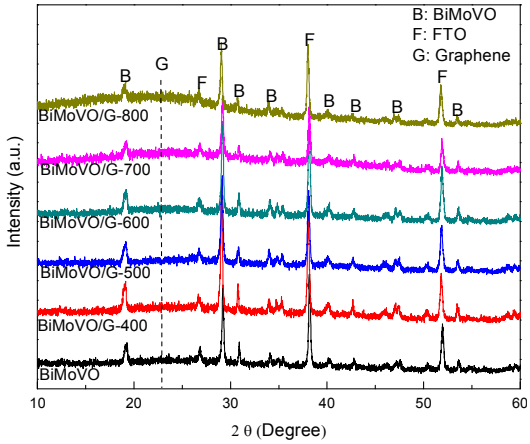

Figure 1. XRD patterns of the prepared BiMoVO and BiMoVO/G composites with different graphene deposition time.

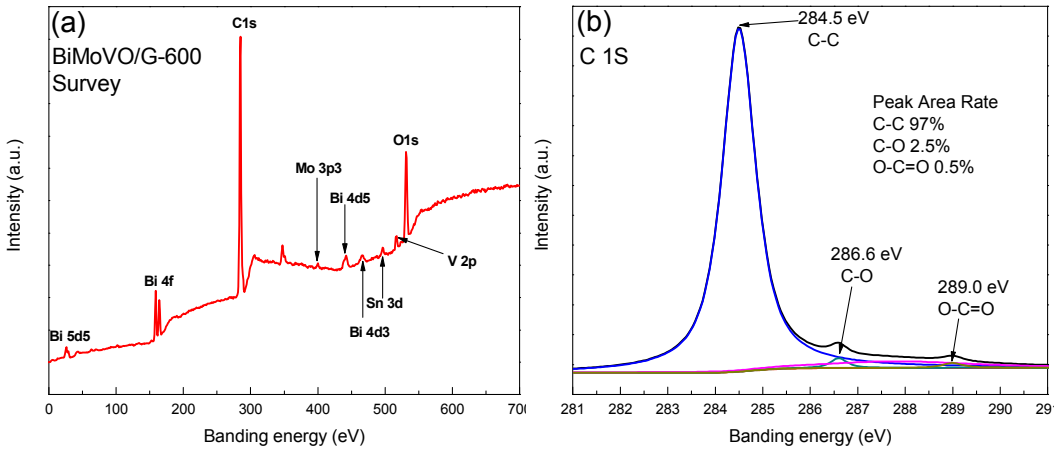

Figure 2. XPS spectra of the BiMoVO/G-600 composite. (a) the total survey spectrum. (b) the C1s XPS core level spectrum.

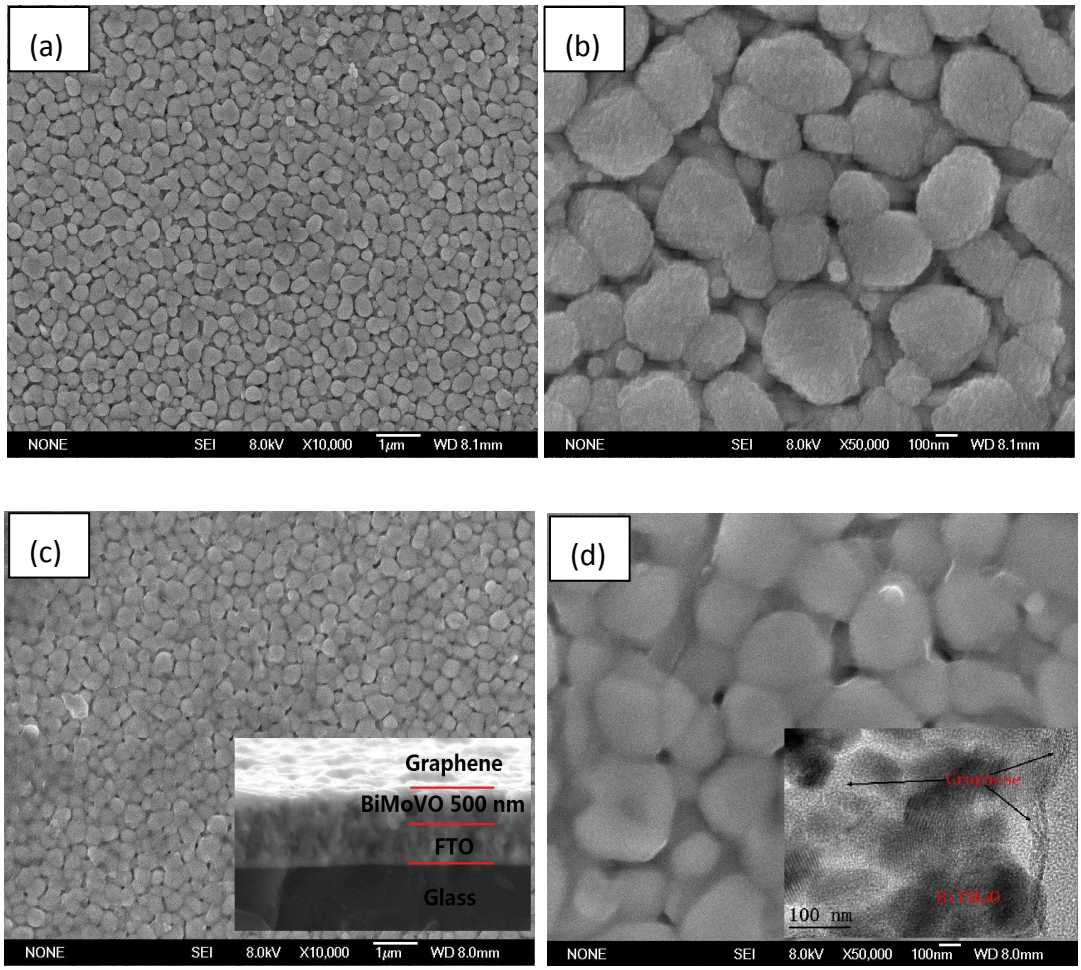

Figure 3. SEM images of the BiMoVO thin film at low (a) and high (b) magnification; and the BiMoVO/G-600 thin film at low (c) (the inset in Figure 3c is the cross-section view of the BiMoVO/G-600 thin film) and high (d) magnification (inset in Figure 3d is the TEM of the BiMoVO/G-600 thin film).

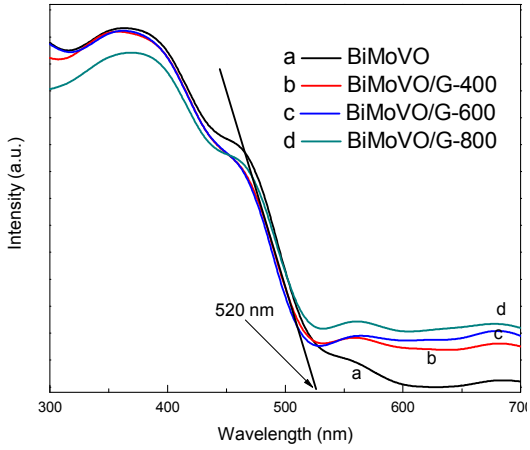

Figure 4. UV/Vis diffuse reflection spectra of (a) BiMoVO; (b) BiMoVO/G-400; (c) BiMoVO/G-600; (d) BiMoVO/G-800.

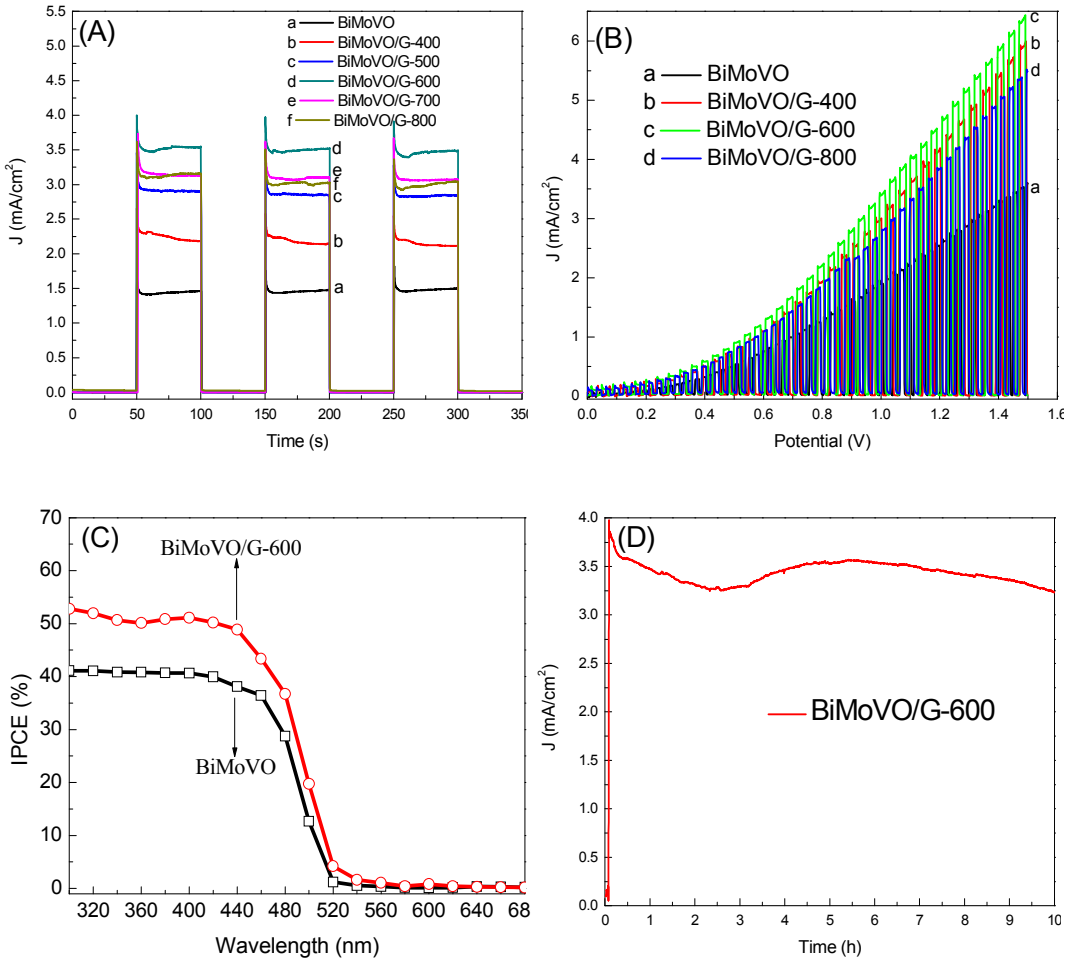

Figure 5. (A) Photoinduced i-t curves of the BiMoVO and BiMoVO/G photoanodes with different graphene deposition time under visible light illumination and at the bias potential of 1 V (vs Ag/AgCl); (B) Photoinduced i-V curves of the BiMoVO, BiMoVO/G-400, BiMoVO/G-600 and BiMoVO/G-800 photoanodes under visible light illumination; (C) The IPCE curves

of BiMoVO and BiMoVO/G-600 photoanodes at the bias potential of 1 V (vs Ag/AgCl); (D) Photoinduced i-t curve of the BiMoVO/G-600 photoanode under a longtime visible light illumination at the bias potential of 1V (vs Ag/AgCl). All of the above mentioned tests were performed in 0.1 M Na_2SO_4 neutral solution.

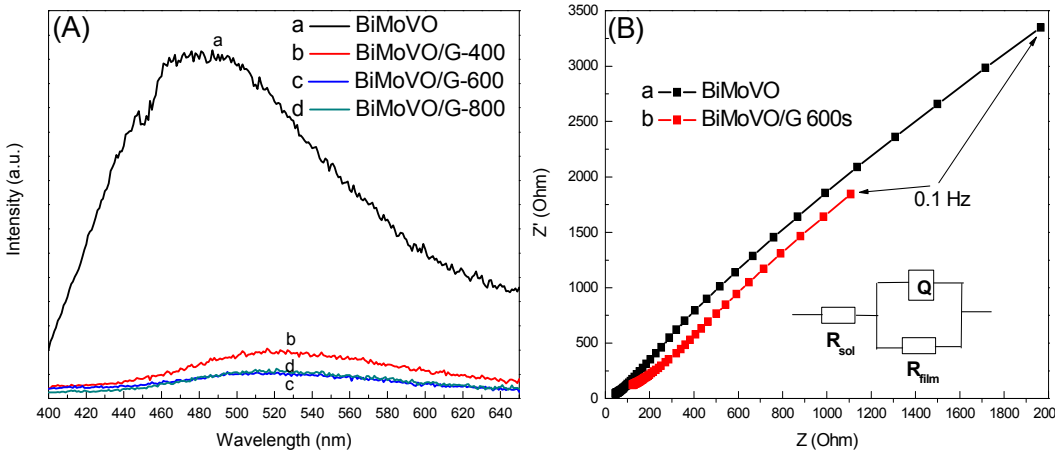

Figure 6. (A) Photoluminescence curves of the BiMoVO, BiMoVO/G-400, BiMoVO/G-600 and BiMoVO/G-800 photoanodes; (B) EIS results of the BiMoVO and BiMoVO/G-600 photoanodes under dark at a frequency range from 10^5 to 10^{-1} Hz in 0.1 M Na_2SO_4 neutral electrolyte.

Table 1. Fitted parameters of the EIS results of the photoelectrodes of BiMoVO and BiMoVO/G-600.

Sample	R_{sol} (Ω cm^2)	R_{film} (Ω cm^2)	Q (Ω^{-1} cm^2 s^n)
BiMoVO	114.38	5017.34	1.23×10^{-4}
BiMoVO/G-600	125.12	3392.27	2.48×10^{-4}

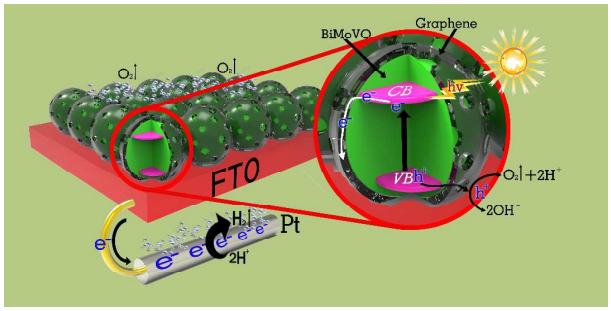

Figure 7. Proposed mechanism for the charge transfer of the photogenerated electrons and holes of the BiMoVO/G thin-film photoanode.

Acknowledgements

This work was financially supported by the National Natural Science Foundation of China (Grant No. 41206067) and The Foundation of Key Laboratory of Marine Environmental Corrosion and Bio-fouling, Institute of Oceanology, Chinese Academy of Sciences.

Notes and references

[a]School of Environment and Safety Engineering, Qingdao University of Science and Technology, 53 Zhengzhou Road, Qingdao 266042, China

[b]Key Laboratory of Marine Environmental Corrosion and Bio-fouling, Institute of Oceanology, Chinese Academy of Sciences, 7 Nanhai Road, Qingdao 266071, China

Corresponding author, Prof. Zhuoyuan Chen; Email: zychen@qdio.ac.cn; Tel: +86-532-82898731; Fax: +86-532-82880498

1 N. Serpone, A. V. Emeline, *J. Phys. Chem. Lett.,* 2012, **3**, 673–677.

2 H. Kisch, *Angew. Chem. Int. Ed*., 2013, **52**, 812–847.

3 L. Zhang, D. Jing, X. She, H. Liu, D. Yang, Y. Lu, J. Li, Z. Zheng, L. Guo, *J Mater. Chem. A*, 2014, **2**, 2071–2078.

4 G. Liu, J. C. Yu, G. Q. Lu, H. M. Cheng, *Chem. Commun*., 2011, **47**, 6763–6783.

5 Y. Y. Bu, Z. Y. Chen, *J. Power Sour.*, 2014, 272, 647–653.

6 K. Maeda, *J. Photochem. Photobiol. C: Photochem. Rev*., 2011, **12**, 237–268.

7 F. Lin, D. Wang, Z. Jiang, Y. Ma, J. Li, R. Li, C. Li, *Energy Environ. Sci*., 2012, **5**, 6400–6406.

8 Q. Liu, J. He, T. Yao, Z. Sun, W. Cheng, S. He, Y. Xie, Y. Peng, H. Cheng, Y. Sun, Y. Jiang, F. Hu, Z. Xie, W. Yan, Z. Pan, Z. Wu, S. Wei, *Nat. Comm*., 2014, **5**, DOI: 10.1038/ncomms6122.

9 K. S. Novoselov, A. K. Geim, S. V. Morozov, D. Jiang, Y. Zhang, S. V. Dubonos, I. V. Grigorieva, A. A. Firsov, *Science*, 2004, **306**, 666-669.

10 A. K. Geim, K. S. Novoselov, *Nat. Mater*. 2007, **6**, 183−191.

11 D. A. Dikin, S. Stankovich, E. J. Zimney, R. D. Piner, G. H. G. Dommett, G. Evmenenko, S. T. Nguyen, R. S. Ruoff, *Nature*, 2007, **448**, 457−460.

12 D. Li, R. B. Kaner, *Science*, 2008, **320**, 1170−1171.

13 H. Chen, M. B. Muller, K. J. Gilmore, G. G. Wallace, D. Li, *Adv. Mater*., 2008, **20**, 3557−3561.

14 H. Zhang, X. Fan, X. Quan, S. Chen, H. Yu, *Environ. Sci. Technol*., 2011, **45**, 5731−5736.

15 C. Liu, Y. Teng, R. Liu, S. Luo, Y. Tang, L. Chen, Q. Cai, *Carbon*, 2011, **49**, 5312−5320.

16 M. Dutta, S. Sarkar, T. Ghosh, D. Basak, J. Phys. Chem. C, 2012, **116**, 20127−20131.

17 Y. Bu, Z. Chen, W. Li, B. Hou, *ACS Appl. Mater. Interfaces*, 2013, **5**, 12361−12368.

18 G. Williams, B. Seger, P. V. Kamat, *ACS Nano*, 2008, 2, 1487−1491.

19 T. Xu, L. Zhang, H. Cheng, Y. Zhu, *Appl. Cata. B: Envireon*., 2011, **101**, 382−387.

20 H. Kim, G. Moon, D. Monllor-Satoca, Y. Park, W. Choi, *J. Phys. Chem. C*, 2011, **116**, 1535−1543.

21 A. Iwase, Y. H. Ng, Y. Ishiguro, A. Kudo, R. Amal, *J. Am. Chem. Soc*., 2011, **133**, 11054–11057.

22 P. Song, X. Zhang, M. Sun, X. Cui, Y. Lin, *Nanoscale*, 2012, **4**, 1800–1804.

23 M. Long, W. Cai, H. Kisch, *J. Phys. Chem. C*, 2008, **112**, 548–554.

24 H. Luo, A. H. Mueller, T. M. McCleskey, A. K. Burrell, E. Bauer, Q. X. Jia, *J. Phys. Chem. C*, 2008, **112**, 6099–6102.

25 K. Sayama, A. Nomura, T. Arai, T. Sugita, R. Abe, M. Yanagida, T. Oi, Y. Iwasaki, Y. Abe, H. Sugihara, *J. Phys. Chem. B*, 2006, **110**, 11352–11360.

26 K. Sayama, N. Wang, Y. Miseki, H. Kusama, N. Onozawa-Komatsuzaki, H. Sugihara, *Chem. Lett*., 2012, **39**, 17–19.

27 I. Akihide, A. Kudo, *J. Mater. Chem*., 2010, **20**, 7536–7542.

28 A. B. Murphy, P. R. F. Barnes, L. K. Randeniya, I. C. Plumb, I. E. Grey, M. D. Horne, J. A. Glasscock, *Int. J. Hydrogen Energy*, 2006, **31**, 1999–2017.

29 S. Cho, H. S. Park, H. C. Lee, K. M. Nam, A. J. Bard, *J. Phys. Chem. C*, 2013, **117**, 23048−23056.

30 W. Luo, Z. Yang, Z. Li, J. Zhang, J. Liu, Z. Zhao, Z. Wang, S. Yan, T. Yu, Z. Zou, *Energy Environ. Sci*., 2011, **4**, 4046–4051.

31 S. J. Hong, S. Lee, J. S. Jang, J. S. Lee, *Energy Environ. Sci*., 2011, **4**, 1781–1787.

32 T. W. Kim, K. S. Choi, *Science*, 2014, **343**, 990-994.

33 Y. Sun, B. Qu, Q. Liu, S. Gao, Z. Yan, W. Yan, B. Pan, S. Wei, Y. Xie, *Nanoscale*, 2012, **4**, 3761–3767.

34 Y. H. Ng, A. Iwase, A. Kudo, R. Amal, *J. Phys. Chem. Lett*., 2010, **1**, 2607–2612.

35 S. Tokunaga, H. Kato, A. Kudo, *Chem. Mater*., 2001, **13**, 4624–4628.